Spectrum Journal of Innovation, Reforms and Development
Volume 43, September 2025 | ISSN (E): 2751-1731
WEBSITE: WWW.SJIRD.JOURNALSPARK.ORG

TREATMENT OF AL-DIWANIYAH REFINERY WASTEWATER USING KARBALA CLAY-BASED CERAMIC MEMBRANES

Adyan Yahya Ghanim 1 ,
H.I.Dawood 2,
Haider Alaa Maabed 3
1,2,3 University of Al-Qadisiyah, College of Engineering
adyan.yahya.ganim@qu.edu.iq 1,
hasan.dawwood@qu.edu.iq 2

Abstract
This study aimed to fabricate and characterize a new flat ceramic membrane using Karbala clay and wood sawdust via a disc casting method for microfiltration applications. The membrane sintered at 1050 °C for 3 hours exhibited a porosity of 53.76%, pore size ≈1.45 µm, and water permeability of 183.76 L/h·m²·bar. Performance evaluation using wastewater from the Al-Diwaniyah refinery under of 1–2 bar, 30–40 °C, and 30–60 L/h flow rate. The results showed that the system achieving up to 96% turbidity removal at 2 bar, 40 °C, and 45 L/h, with a moderate reduction in Chemical Oxygen Demand (COD) and Total Dissolved Solids (TDS). The treated water pH increased from 7.4 to 8.1, indicating alkalinity interactions with the ceramic surface. These findings demonstrate that locally fabricated ceramic membranes provide a cost-effective and eco-friendly solution for industrial wastewater treatment, with potential for further design optimization.

Keywords: Karbala clay, Sawdust, Ceramic membrane, Microfiltration, Industrial wastewater treatment, Al-Diwaniyah refinery.

Introduction

Water pollution is one of the most critical environmental challenges caused by industrial, agricultural, and urban expansion. Wastewater typically contains complex contaminants such as heavy metals, synthetic dyes, oils, nutrients, and pathogenic microorganisms, which are difficult to remove using conventional methods such as sedimentation, coagulation, and biological treatment. Therefore, membrane technologies have emerged as promising alternatives due to their high selectivity and effective separation performance. Although polymeric membranes such as polyvinylidene fluoride, polyether sulfone, and polyacrylonitrile are widely applied, their limited thermal and mechanical stability, along with rapid fouling, reduces their efficiency in treating complex industrial wastewater. This has significant attention toward ceramic membranes prepared from natural clay and sawdust, which offer chemical, thermal, and mechanical stability along with their low cost.

Operating pressure is one of the most influential parameters affecting the performance of ceramic membranes, as it directly controls water flux, separation efficiency, and the rate of pore blockage. [1] reported that increasing pressure from 1 to 2.5 bar significantly enhanced flux, while [2] showed that 1.5 bar represented an optimal balance between higher flux and reduced fouling. [3]observed that operating above 2 bar accelerates pore blockage. [4] found that a lower pressure of 1.2 bar was sufficient for organic matter removal, [5] indicated that the range of 1–1.5 bar is most suitable for clay-based membranes.

In addition, operating temperature serves as a critical factor in improving permeability and reducing fouling, as it affects water viscosity, enhances flux, and mitigates organic and microbial deposition on the membrane surface. [6] demonstrated that raising feed temperature from 25 to 50 °C increased flux by nearly 30%. [7] reported that operation at 30–60 °C enhanced dye removal and reduced fouling. [8] confirmed that increasing the operating temperature up to 50 °C improved removal efficiency without compromising structural stability. [9] showed that moderate heating facilitated the removal of heavy organic compounds, [10] cautioned that sudden thermal fluctuations may cause membrane cracking, highlighting the importance of gradually increasing the temperature operation.

Furthermore, flow rate is an important operational parameter, although its impact is comparatively less significant than that of pressure and operating temperature, as it governs concentration polarization and cake layer formation on the membrane surface, thereby indirectly influencing filtration efficiency and membrane stability. [11] applied a continuous flow of 25 Liter/hour (L/h), which prevented fouling and ensured effective bacterial removal. [12] maintained a steady flow of 30 L/h, which improved water distribution and reduced fouling. [13] achieved stable performance at 20 L/h with minimal fouling, [14] demonstrated that alternating flow between 22–35 L/h generated shear stress that minimized deposits. [15] highlighted that gradually increasing flow up to 60 L/h maintained high filtration efficiency and reduced the risk of mechanical damage.

Based on these reviewed findings, this study aimed to address the research gap by developing a novel ceramic microfiltration membrane using local Karbala clay, which has not been previously explored in membrane fabrication studies. Karbala clay was selected due to its abundance, low cost, and favorable mineralogical properties, as well as its symbolic and cultural significance to the region. The disc-shaped membrane was fabricated and evaluated under typical operating conditions of pressure, temperature, and flow rate. The results confirmed its potential as an effective, sustainable, and economically viable material for water treatment applications.

2. Experimental Procedure

2.1. Raw Materials

In this study, natural clay obtained from Karbala province (Iraq) was used as the primary raw material for the fabrication of ceramic discs, without undergoing any chemical pretreatment. Clay minerals are widely used in ceramic processing due to their plasticity, availability, and favorable composition, as previously discussed [16]. The raw clay was air dried at ambient temperature until it reached adequate rigidity for milling. It was then pulverized using an electric grinder, and the finest powder naturally obtained from the grinding process was selected for disc formation, without additional sieving. The particle size of the selected clay powder was estimated based on imaging analysis using a scanning Electron Microscope (SEM) (Model:

Thermo Scientific Apreo S, Manufacturer: Thermo Fisher Scientific, USA), which revealed ultrafine particles with an average diameter of approximately 10 µm.

To improve the structural characteristics and enhance porosity of the ceramic matrix, wood sawdust was introduced as a pore forming agent. The sawdust was produced using an electric grinding machine, then manually sieved in the laboratory using a standard 60 mesh sieve (corresponding to a particle size of approximately 60 µm), ensuring uniformity in the pore former particle size. [17] reported that the use of sawdust with controlled particle size effectively influences porosity and pore size distribution in low cost ceramic membranes.

2.2. Fabrication of the Ceramic Disc

A ceramic disc with dimensions of 5 cm in diameter and 0.5 cm in thickness was fabricated employing a shaping technique suitable for small scale laboratory processing. The solid phase comprised a binary mixture consisting of 80 wt% raw clay soil (collected from Karbala province) and 20 wt% wood sawdust as a pore forming agent. The dry powders were manually blended using a laboratory spatula for 10 minutes until a visually homogeneous mixture was achieved. Following dry mixing, deionized water was gradually incorporated at 40 wt% relative to the total mass (solids + water) to produce a plastic paste appropriate for molding. The mixture was allowed to rest for approximately 15 minutes to ensure adequate moisture distribution and enhance particle interaction. The resulting paste was shaped into a disc using a simple mold based forming technique. The formed samples were dried under controlled ambient conditions, followed by sintering in a programmable furnace under optimized parameters to achieve ceramic consolidation. The drying and sintering processes applied to the shaped ceramic discs are described in detail in next section.

2.3. Thermal Program

Thermal treatment is a fundamental step in the fabrication of ceramic supports, directly affecting their physical integrity and structural properties. In this study, the thermal program consisted of two main stages: drying and sintering, as illustrated in the thermal treatment diagram (Fig. 1).

This multi stage heating profile aligns with established ceramic processing Protocols, which recommend gradual ramping to achieve mechanically stable porous structures (Reed, 1995).

Drying was performed at 100 °C for 4 hours (h) with a heating rate of 2 °C/min in a vacuum oven (Model: VO-64, 220V, 1.5 kW, Max Temperature: 200 °C; Manufacturer: South Korea). Sintering was subsequently conducted in a programmable muffle furnace (Model: JSMF-14 GT, Manufacturer: JSR, South Korea). The sintering process included heating to 500 °C at 5 °C/min and holding for 3 h to burn out organic pore forming agents, followed by heating to 1050 °C at the same ramp rate and holding for 3 h to promote ceramic densification and structural stability. These stages were performed on separate days to ensure gradual temperature increases, minimizing thermal stresses and crack formation.

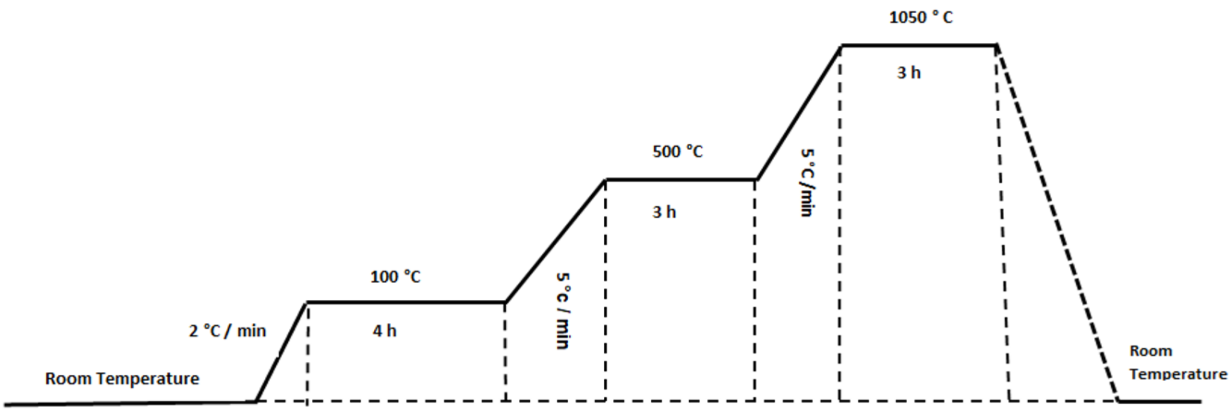

Fig. 1. Thermal treatment profile applied to the ceramic membrane.

2.4. Filtration System Components

Fig. 2 shows the photographic view of the Filtration System Components. The filtration system used in this study consists of several main components, including commercially sourced parts, locally available materials, and custom-fabricated elements designed specifically for this setup.

The system begins with a transparent cylindrical feed tank made of acrylic, 20 cm in diameter and 26 cm in height, serving as the primary reservoir for the feed solution. Two 10-inch polypropylene pre-filters, manufactured in China, were installed to remove large suspended solids before the solution reaches the pumping unit.

The system employs two reinforced diaphragm pumps of the COBRA ECO 100 GPD type, also manufactured in China, each capable of generating a maximum pressure of 6.8 bar. The pumps were connected in parallel to ensure stable and continuous flow.

Flow rate was controlled using a variable area flow meter (rotameter) imported from China. This vertical, transparent device features a floating indicator for direct readings, covering a measuring range from 20 to 100 L/h. A digital thermometer (model TP101, made in China) was used to monitor the water temperature during operation. It includes a stainless-steel probe and an LCD screen, with a measurement range from −50 to 300 °C.

Operational pressure was monitored using two analog pressure gauges (manufactured in China). The first gauge measures 0–10 bar, while the second covers 0–7 bar. Both were connected in series to accurately measure the pressure drop across the membrane.

High quality white polyvinyl chloride tubing was used to connect the hydraulic components, along with several manual ball valves for start/stop control. A main control valve was installed before the rotameter to adjust the total flow rate.

The system includes a horizontal stainless-steel pressure vessel, 25 cm in diameter and 36 cm in height, holding a flat ceramic membrane disc of 5 cm diameter and 0.5 cm thickness, designed to ensure full contact with the feed water.

Finally, a recirculation loop was incorporated to connect the outlet of the pressure vessel back to the feed tank, enabling continuous solution circulation and contributing to thermal and hydraulic stability during operation.

Fig. 2 Photographic view of the filtration system.

2.5. Flow Path and Filtration System Operation

The filtration process begins with the introduction of contaminated industrial wastewater, collected from the Al-Diwaniyah Oil Refinery, into a transparent cylindrical feed tank. The water is then transferred to two primary filters to remove large solid particles, and then pumped by two pumps connected in parallel to ensure a continuous flow. The flow rate is regulated between 30 and 60 L/h using a main control valve, while the pressure is adjusted within a range of 1 to 2 bar. The operating temperature ranges from 30 to 40°C. Operating conditions are monitored using pressure gauges, a flow meter, and a mercury thermometer.

After adjusting the parameters, the water is directed to a steel tank containing a horizontally mounted ceramic membrane, where the final filtration process takes place. The pure water is separated from the contaminants across the membrane surface, and the resulting permeate is collected in the outlet pipe for analysis. The unfiltered portion is returned to the feed tank to ensure continuous circulation and maintain stable conditions throughout the 30-minute experiment. These experiments aimed to evaluate the membrane's efficiency in reducing four key water pollution indicators: COD, TDS, turbidity, and pH. The concentration of each pollutant was recorded before and after filtration.

The rejection ratio (R) was calculated using the following equation Eq. (1), as reported [18]:

$$R = \frac{C_{Feed} - C_{permeate}}{C_{Feed}} \times 100 \quad (1)$$

Where:

C_{feed}: Concentration of the contaminant in the feed water.

$C_{permeate}$: Concentration of the contaminant in the treated (permeate) water.

In addition to rejection efficiency, the hydraulic performance of the ceramic membrane was assessed by calculating the permeate flux J (L/h·m^2) and hydraulic permeability Lp (L/h·m^2·bar), as described [19] using the following equations Eq. (2) and Eq. (3):

$$J = \frac{V}{A.\Delta t} \quad (2)$$

$$Lp = \frac{J}{\Delta P} \quad (3)$$

Where:

V= Volume of permeate collected during filtration (L).

A= Effective surface area of the membrane, calculated based on the membrane geometry (e.g., for a flat disc: $A = \pi r^2$) (m^2).

Δt= Filtration time (h).

ΔP = Transmembrane pressure difference (bar).

It is noteworthy that no cleaning procedures were performed on the membrane during the operational period, with the aim of evaluating its efficiency and resistance to fouling accumulation under controlled operating conditions. This approach was adopted to study the operational durability of the ceramic membrane without external interventions.

2.6. Characterizations Techniques

A series of standard characterizations was conducted to evaluate the physical, chemical, thermal, and structural properties of the raw materials (clay and sawdust) as well as the fabricated ceramic membrane. The elemental composition of the raw clay was analyzed using Energy Dispersive X-ray Spectroscopy (EDX) system (Model: Shimadzu, Manufacturer: Shimadzu Corporation, Japan), which enabled the qualitative and semi-quantitative identification of both major and trace elements. The mineralogical phases of the raw clay were identified using X-ray Diffraction

(XRD) (Model: Bruker D8 Advance, Manufacturer: Bruker Corporation, USA), which facilitated the detection of crystalline structures within the material.

The thermal behavior of the raw clay and sawdust was assessed using Thermogravimetric Analysis (TGA) and Differential Thermal Analysis (DTA), performed with a LABSYS EVO 1F device (SETARAM, France) in an air atmosphere over a temperature range from room temperature to 1000 °C, at a constant heating rate of 5 °C/min, to monitor mass loss and thermal transitions.

The surface morphology of the powdered clay and the sintered ceramic membrane was examined using SEM. The pore size of the membrane layer was determined from the SEM images using Image J software (Version 1.44e), providing insight into the microstructure, particle shape, and pore distribution.

In addition to evaluating membrane performance, the physical properties of the ceramic membrane including open porosity, water absorption, and bulk density were determined based on the Archimedes method, following the ASTM C373-88 standard. The procedure involved measuring the membrane's weight in three conditions: dry, suspended in water, and saturated: dry (m_dry), suspended in water (m_wet), and saturated (m_sat). These values were used to calculate the properties using the following equations Eq. (4 - 6), as described [20] and [21]:

$$Porosity = \frac{m_{sat} - m_{dry}}{m_{sat} - m_{wet}} \times 100 \quad (4)$$

$$Water\ Absorption = \frac{m_{sat} - m_{dry}}{m_{dry}} \times 100 \quad (5)$$

$$Bulk\ Density\ \left(\frac{g}{cm^3}\right) = \frac{m_{dry}}{m_{sat} - m_{wet}} \quad (6)$$

Where:

m_{sat}: Saturated mass of the membrane after immersion and gentle surface wiping to remove excess water (g).

m_{dry}: Dry mass of the membrane after oven drying at 110 °C for 24 h (g).

m_{wet}: Suspended mass of the membrane while hanging in water (g).

Furthermore, the pH and TDS of feed and permeate samples were measured using Lovibond TB 300 IR (Lovibond, TB 300 IR; equipped with digital keypad, LCD display, and suitable for multi-parameter IR analysis). The turbidity of water samples before and after filtration was analyzed using HACH 2100Q Portable Turbidimeter. COD was determined using Lovibond Checkit Direct COD VARIO, which allows direct measurement with an LCD display and pre-calibrated reagents).

This comprehensive characterization approach provides accurate insights into the structural integrity, microstructural features, and performance of the fabricated ceramic membrane under different operational conditions.

Results and Discussion

Characterization of Raw Karbala Clay Powder

3.1.1 EDX Analysis

The chemical composition of the raw Karbala clay expressed in mass percentages (wt.%) of the elements is presented in Table 2. The results revealed that the clay is mainly composed of high amounts of silicon (39.055%), calcium (27.556%), iron (14.130%), and aluminum (13.718%). These four elements constitute the major components of the raw clay, representing nearly 94% of the total composition, which explains the distinctive physical and mechanical properties of this natural clay.

The Si/Al mass ratio was calculated to be approximately 2.85, clearly indicating that Karbala clay belongs to the family of aluminosilicates [22], which are well known for their high thermal endurance and suitability for ceramic processing.

In addition, small amounts of trace elements such as potassium (2.768%), titanium (1.401%), and sulfur (0.202%) were detected, along with very minor concentrations of manganese (0.263%), chromium (0.089%), nickel (0.074%), vanadium (0.060%), zirconium (0.046%), copper (0.044%), zinc (0.044%), and yttrium (0.011%). Although present in low proportions, these trace elements play a significant role in enhancing sintering behavior and improving the chemical and thermal stability of the material.

Table 1. Elemental composition of raw Karbala clay determined by EDX analysis

Element	Composition (%)
Si	39.055
Ca	27.556
Fe	14.130
Al	13.718
K	2.768
Ti	1.401
S	0.202
Mn	0.263
Cr	0.089
Ni	0.074
V	0.060
Zr	0.046
Cu	0.044
Zn	0.044
Y	0.011

3.1.2 XRD Analysis

XRD analysis was conducted on the raw Karbala clay sample to determine its mineralogical composition before any thermal treatment. The resulting diffractogram is shown in Fig. 3 and reveals the presence of several primary and secondary crystalline phases. The primary phases, representing the main mineral structure of the clay, include kaolinite (K) at $2\theta = 12°$ and quartz (Q) at $2\theta = 26°$. The secondary phases, which contribute to the mechanical and thermal properties of the clay, include vermiculite (V) at $2\theta = 14°$, muscovite (M) at $2\theta = 22°$ and 51°, dolomite (D) at $2\theta = 34°$, albite (A) at $2\theta = 40°$, hematite (H) at $2\theta = 63°$, rutile (R) at $2\theta = 75°$, and anatase (An) at $2\theta = 82°$.

These results highlight the heterogeneous crystalline distribution of the raw clay, reflecting its natural composition and suitability for producing ceramic membranes with stable mechanical and thermal properties. Similar results have been reported for comparable natural clays [22].

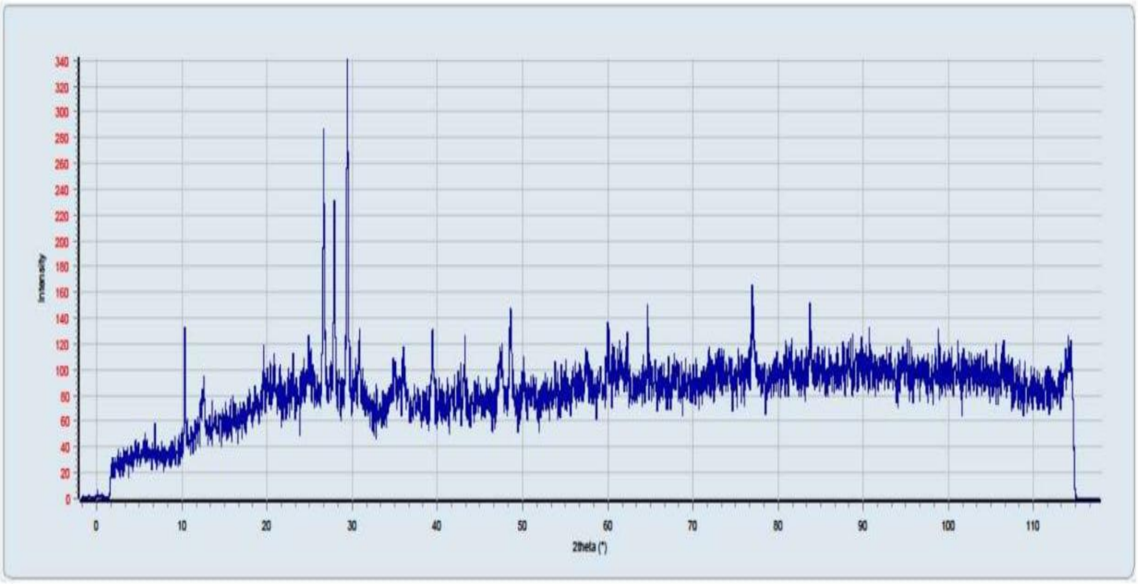

Fig. 3 XRD pattern of raw Karbala clay.

3.1.3 Thermal Analysis

The thermal behavior of a raw clay and wood sawdust mixture was investigated using TGA and DTA over a temperature range from room temperature to 1000 °C, as illustrated in Fig. 4.

The TGA curve exhibited a minor initial weight loss below 200 °C, attributed to the evaporation of free and physically adsorbed water from the clay matrix and the hygroscopic sawdust particles. A major decomposition stage occurred between 200 °C and 770 °C, resulting in a substantial weight loss of approximately 83%. This loss is primarily associated with the thermal degradation of lignocellulosic components in the wood sawdust and the breakdown of thermally unstable clay minerals. The corresponding DTA curve displayed a pronounced exothermic peak around 770 °C, indicating combustion of organic matter and structural transformations within the composite material. Additionally, the first derivative of the TGA curve revealed a weight loss rate of 0.8% per minute during this phase, reflecting rapid thermal degradation kinetics and confirming the active decomposition behavior of the mixture.

These results are consistent with previous findings [23] who reported that the inclusion of wood sawdust in clay composites significantly affects their thermal decomposition profile, enhancing organic burnout and increasing the porosity of the final ceramic structure. The current observations further support the applicability of such clay-sawdust mixtures in high temperature ceramic processes.

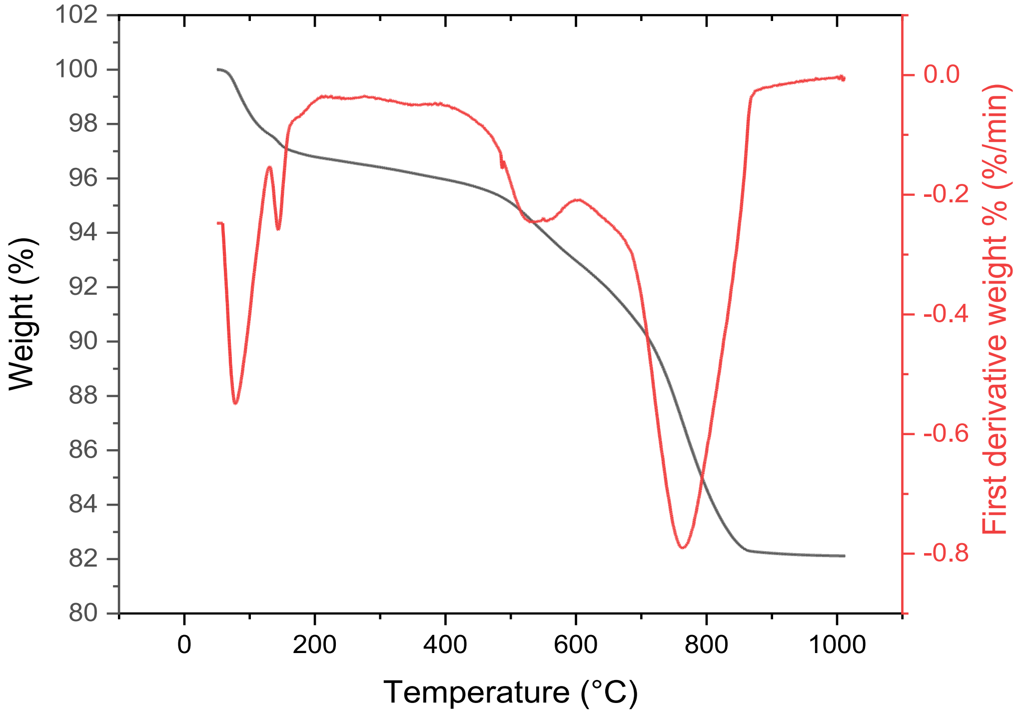

Fig. 4 Thermo-analytical Curves of Karbala Clay and Wood Sawdust.

3.1.4 Microstructural Analysis:

The SEM micrograph of the raw Karbala clay (Fig. 5) reveals a heterogeneous morphology with irregularly shaped particles and rough surfaces. Primary agglomerates are clearly visible, and small voids between particles indicate the presence of initial porosity prior to sintering. The absence of sintering necks confirms that thermal consolidation has not yet occurred, reflecting the intrinsic microstructure of the clay. Such observations are in agreement with previous studies on clay-biomass composites, which report similar particle heterogeneity and pre-sintering porosity [24].

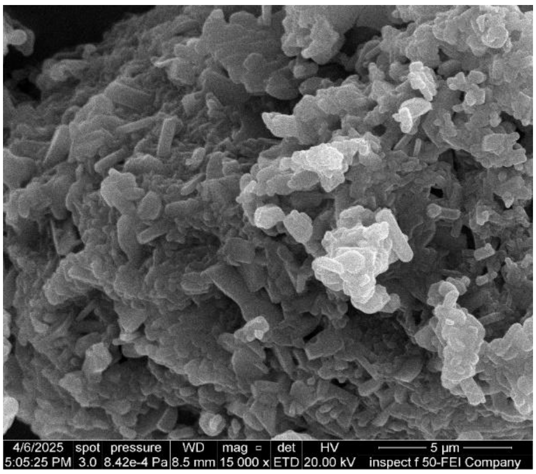

Fig. 5 SEM micrograph of the Karbala clay sample before sintering.

3.2 Characterization of the Karbala Clay Membrane

3.2.1 Visual Appearance of Flat Membranes

Fig. 7 illustrates the visual appearance of Karbala clay-based membranes before and after sintering at 1050 °C. The green, unsintered membrane exhibits a homogeneous surface and a well-defined flat circular shape, with no visible cracks or major defects, indicating uniform particle distribution and effective mixing with sawdust. After sintering, the membrane surface changes to dark brown with the appearance of fine spots, reflecting the onset of glazing and the formation of fine porosity within the structure. This color transformation is associated with the oxidation of iron oxides and phase transitions in the clay minerals during thermal treatment, as well as the combustion of organic sawdust contributing to pore formation and color distribution [25]. A slight dimensional shrinkage is also observed due to thermal contraction, confirming the development of the microstructure and increased structural density of the membrane.

Fig. 7 Views of Karbala clay-sawdust membrane: (a) unsintered membrane and (b) membrane sintered at 1050 °C.

3.2.2 Porosity, Water Absorption and Bulk Density

The porosity, water absorption, and bulk density of the fabricated ceramic membrane were significantly affected by the sintering process at 1050 °C. The porosity reached 53.76%, indicating a well-developed and interconnected porous framework, which facilitates the passage of water and larger dissolved species. This porous structure can be attributed to the decomposition of organic matter in the sawdust during sintering, which promoted the formation of a continuous pore network within the clay matrix, thereby enhancing the membrane's filtration performance [26]. The water absorption of the membrane was measured at 61.24%, consistent with the high porosity and reflecting the membrane's capacity to retain water within its internal structure. This characteristic improves filtration efficiency and supports its application in microfiltration processes. In contrast, the bulk density was relatively low, at 0.8 g/cm^3, demonstrating the inverse relationship between porosity and density typically observed in ceramic materials, and confirming the formation of a homogeneous and effective porous structure [27]. Furthermore, the presence of natural oxides in Karbala clay, such as MgO, K_2O, and Na_2O, contributes to partial glazing and stabilization of the pore network, enhancing the structural integrity of the membrane while maintaining high water absorption, thus ensuring its mechanical durability during operation [28]. Overall, these results indicate that the fabricated membrane combines high porosity, adequate water absorption, and structural stability, making it suitable for both microfiltration and industrial applications. The obtained values are consistent with the microscopic features observed in SEM images, confirming the formation of a connected and uniform porous network capable of supporting practical membrane performance.

3.2.3 Surface and Cross-Sectional Morphology

Fig. 8 SEM micrograph of the surface and cross section of the ceramic disc sintered at 1050 °C. According to the SEM observations, the ceramic disc exhibits a homogeneous morphology with a relatively smooth surface, well distributed pores, and no visible cracks or structural imperfections. The pore size of the membrane was estimated to be 1.45 µm, which clearly falls within the microfiltration range. This value was directly obtained from SEM micrograph analysis, following the methodology reported [29], who applied digital image analysis to characterize the pore structure and size distribution of ceramic membranes.

The porous network in the disc originates from the combustion of the lignocellulosic components of sawdust during sintering, leading to controlled porosity while maintaining a relatively dense microstructure. At the sintering temperature of 1050 °C, SEM micrograph reveal evident grain growth and densification, resulting in smoother surfaces and narrower pore walls compared to membranes treated at lower temperatures. Despite its relatively high porosity, the fabricated disc demonstrated sufficient mechanical robustness, indicating that the selected clay sawdust ratio and the applied sintering schedule successfully achieved a balance between pore formation and structural integrity.

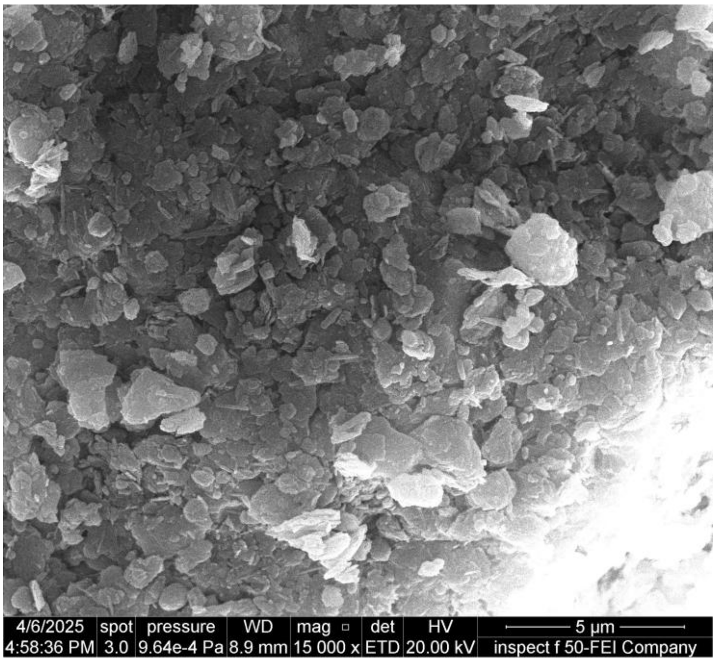

Fig. 8 SEM micrograph of the inner surface of the disc membrane after sintering.

3.3. Filtration Test

The performance of the ceramic membrane fabricated from Karbala clay and wood sawdust was evaluated at a sintering temperature of 1050 °C using industrial water obtained from Al-

Diwaniyah Refinery, with its physicochemical properties summarized in Table 2. Three dimensional surface plots were employed to illustrate the effects of operational parameters pressure, temperature, and flow rate on membrane performance, where Figs. 9a–c represent permeate flux behavior, and Figs. 10a–c indicate turbidity removal efficiency.

Table 2. Physicochemical properties of industrial water from Al-Diwaniyah Refinery

Characteristics	Value
pH	7.41
COD (ppm)	380
TDS (ppm)	3420
Turbidity (NTU)	78.8

3.3.1 Permeate Flux

From the 3D surface plots (Fig. 9a), the surface shows a steep decline along the pressure axis with a slight inclination toward temperature, indicating that pressure is the dominant factor affecting permeate flux. The maximum flux of 367.53 L/h·m² was achieved at 2 bar. This is explained by pressure acting as the primary driving force pushing water through the membrane pores according to Darcy's law [30], while temperature serves as a secondary role by reducing water viscosity and facilitating flow [31].

In Fig. 9b, the surface exhibits a gradual curvature toward pressure, while the slope along the flow rate axis remains nearly constant and fluctuating, indicating that pressure continues to dominate flux behavior. Flow rate mainly contributes to reducing surface fouling without altering the primary driving force [32].

Fig. 9c shows a gradual decline along the temperature axis at constant pressure, while the effect of flow rate remains weak and irregular, reflecting the role of temperature in enhancing flux by lowering water viscosity, making it the controlling factor in this case [31]

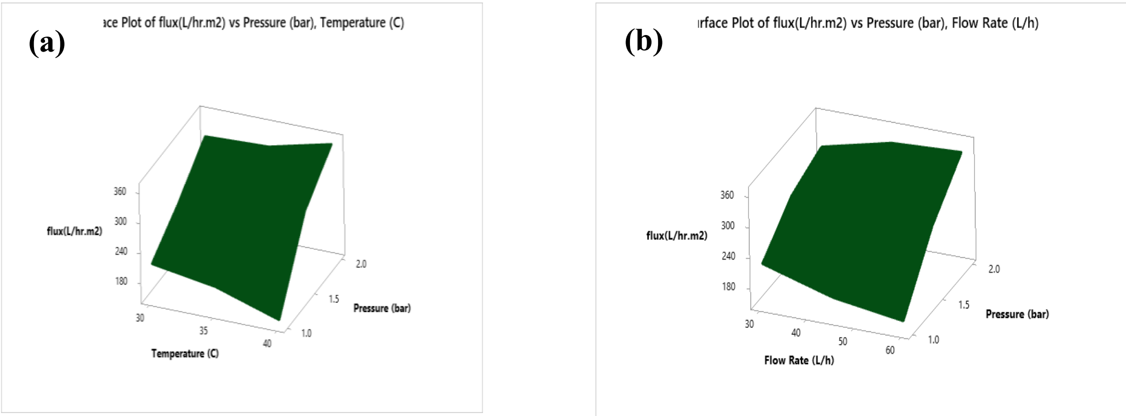

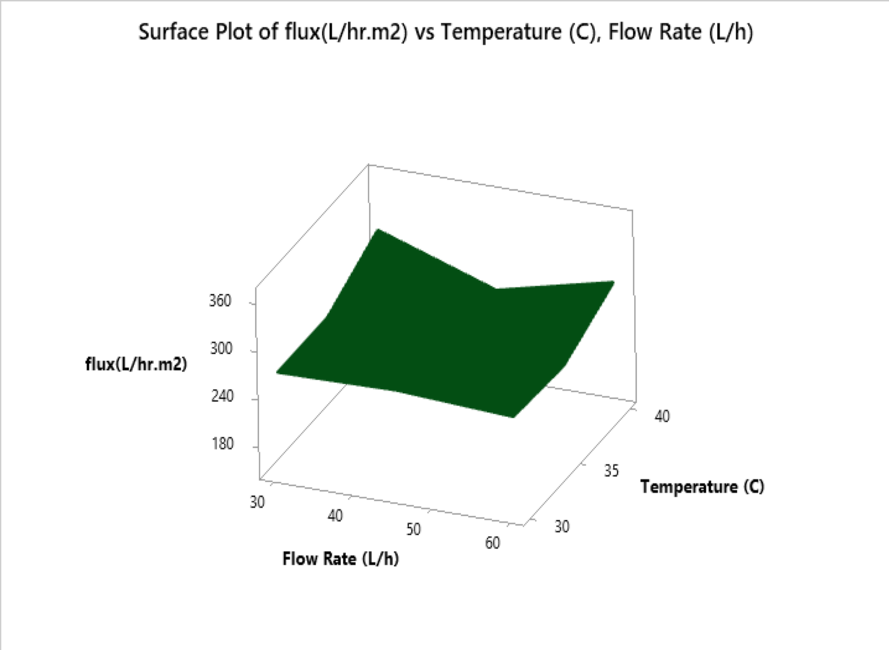

Fig. 9 3D surface plots of permeate flux: (a) effect of pressure and temperature at constant flow rate, (b) effect of pressure and flow rate at constant temperature, (c) effect of temperature and flow rate at constant pressure.

3.3.2 Turbidity Removal Efficiency

From the 3D surface plots (Fig. 10a), the surface slope is toward pressure with a slight curvature toward temperature, confirming that pressure is the dominant factor for turbidity removal, with a maximum efficiency of 96% at 2 bar. This is attributed to the increased driving force and formation of a cake layer on the membrane surface that retains suspended particles [33].

Fig. 10b shows a gradual rise along the pressure axis while remaining nearly flat along the flow rate axis, demonstrating the continued dominance of pressure on removal efficiency. Flow rate only reduces particle accumulation without affecting the primary filtration mechanism [34].

Fig. 10c exhibits a gradual decline along the temperature axis with minimal influence from flow rate, indicating that temperature becomes the controlling factor at constant pressure due to reduced water viscosity and enhanced passage of particles through fine pores [35].

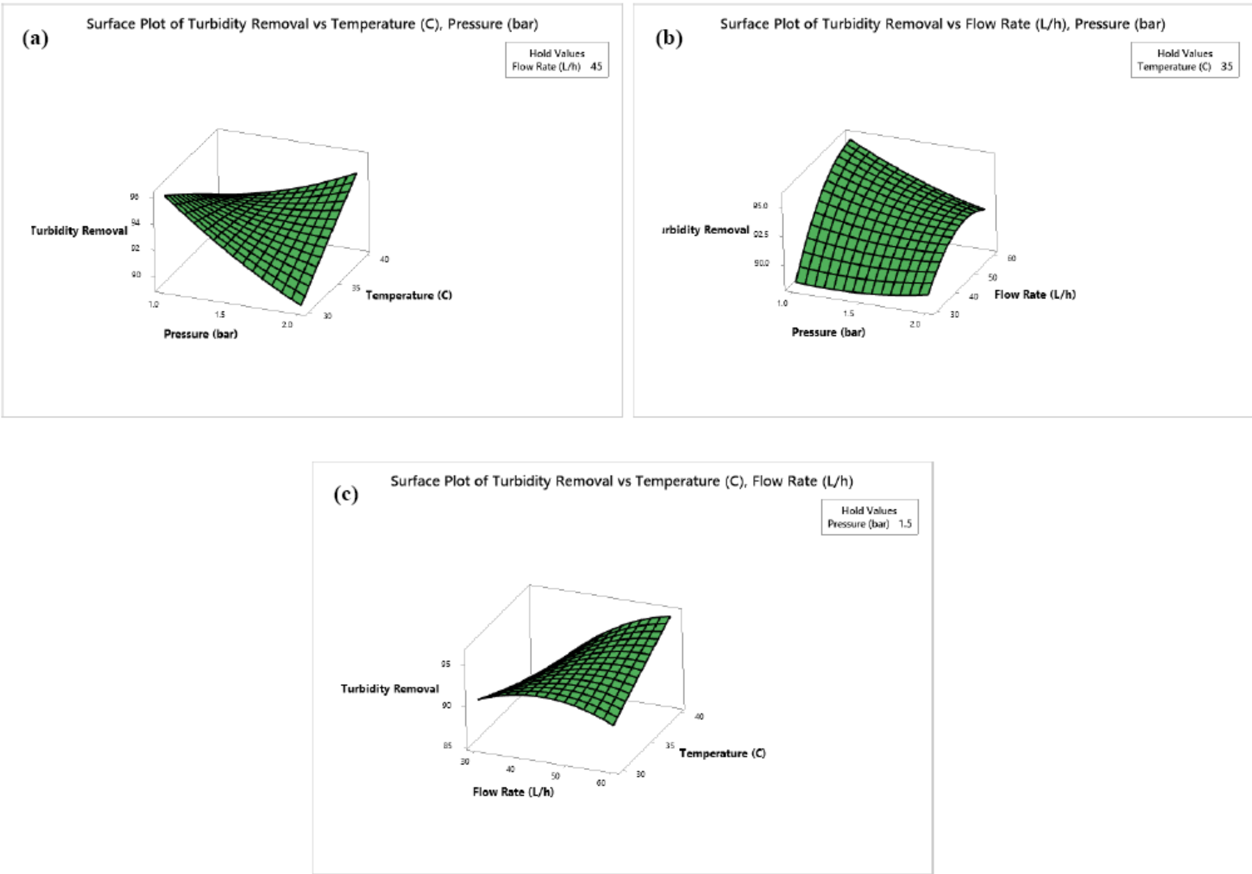

Fig. 10 3D surface plots of turbidity removal: (a) effect of pressure and temperature at constant flow rate, (b) effect of pressure and flow rate at constant temperature, (c) effect of temperature and flow rate at constant pressure.

These 3D surface plots indicate that pressure is the dominant factor for both flux and turbidity, while temperature serves as a secondary role, and flow rate has a limited and fluctuating effect.

The membrane also exhibited limited removal of dissolved components such as COD and TDS, which are small molecules that easily pass through the fine membrane pores, consistent with the characteristics of conventional ultrafiltration membranes. [36] reported that low-cost ceramic membranes show limited performance in removing dissolved pollutants such as COD and TDS due to the permeability of these species through fine pores without an effective retention mechanism.

A slight increase in permeate pH from 7.41 to 8.1 was observed, attributed to the membrane's effect on alkaline constituents and its ion-exchange capability [37]. As shown by the membrane, when compared with other low-cost ceramic membranes (Table 3), the Karbala clay sawdust membrane exhibited high and stable permeability under low pressure, suitable pore size for fine filtration, and high turbidity removal efficiency, making it suitable as a primary stage for industrial water treatment. Furthermore, the removal of dissolved components such as COD and TDS can be enhanced through surface modifications, which increase adsorption capacity and

improve overall performance, making the membrane a promising option for efficient industrial water treatment [38].

Table 3. Characteristics of the Karbala clay membrane compared with those of other membranes made from low-cost materials

Membrane materials	Sintering temperature (C°)	Porosity (%)	Pore size (µm)	Permeability (L/h. m^2. bar)	Feed Turbidity (NTU)	Applied Pressure (bar)	Rejection (%)	Reference
Natural Moroccan clay and phosphate	1100	28.11	2.5	928	Tannery beam house effluent (760) Raw seawater (120) Synthetic solution of aluminum chloride (at high pH) (725)	0.14	99.80 99.62 99.86	[39]
Natural kaolin clay	1250	27	0.73	20	Cuttlefish effluent (335)	3	99	[40]
Natural Moroccan perlite	950	52.11	1.70	1433.46	Agro-food effluent (224) Tannery effluent (36)	0.12	97 96	[41]
Mineral coal fly-ash	800	51	0.25	475	Textile dye wastewater (45.5)	1	98.72	[42]
Natural Karbala clay	1050	53.76	1.45	183.76	Industrial effluent (78.8)	2	96	This work

3.4. Membrane Cost Estimation

The efficient implementation of membrane technology on an industrial scale strongly depends on the manufacturing cost. According to several reported estimates, commercial ceramic membranes range from 500 \$/m² for alumina to 3000 \$/m² for stainless steel [43]. In contrast, polymer membranes are reported to cost between 50 \$/m² and 200 \$/m² [44]. Due to their lower operating costs, ceramic membranes are more advantageous and preferred over polymer membranes under harsh operating conditions for wastewater treatment. In terms of mechanical, chemical, biological, and thermal properties, ceramic membranes also provide lower operating costs and longer service life than polymer membranes.

In the present study, the membranes were fabricated entirely from natural Karbala clay combined with sawdust as a pore-forming agent, both locally available at negligible cost. The membranes were sintered at 1050 °C, which is significantly lower than the temperature required for commercial alumina membranes (above 1200 °C) and those prepared from pure oxides such as Al_2O_3, TiO_2, and ZrO_2. The total preparation cost of the flat ceramic membranes was estimated solely based on electricity consumption. The furnace was operated for 3 hours at a rate of 10,000 Iraqi Dinars per hour, resulting in a total energy cost of 30,000 Iraqi Dinars for the production of five membranes. Accordingly, the cost per membrane was 6,000 Iraqi Dinars, corresponding to approximately 4.22 \$/m^2 based on the current exchange rate (1 \$ = 1,423 IQD).

These cost estimates clearly demonstrate that ceramic membranes fabricated from Karbala clay and sawdust are highly competitive compared to commercial ceramic membranes. The significant reduction in cost is attributed to the use of low-cost, locally available raw materials and the lower sintering temperature. Therefore, the developed membranes represent an economical and sustainable option for industrial water treatment applications, particularly under harsh operating conditions, while maintaining adequate mechanical and chemical stability.

4. Conclusion

In this study, flat ceramic microfiltration membranes were successfully prepared from a mixture of Karbala clay and wood sawdust by disc casting and sintering at 1050 °C for 3 h. The membranes exhibited a porosity of 53.76%, a pore size of 1.45 µm, and a water permeability of 183.67 L/h·m²·bar. SEM analysis confirmed that the membranes were homogeneous, well adhered, and free of cracks. The prepared membranes demonstrated good performance in treating Al- Diwaniyah refinery water, reducing turbidity to 3.15 Nephelometric Turbidity Units (NTU), while COD and TDS removal efficiencies were limited. The preparation cost was approximately 4.22 $/m², highlighting their economic advantage. These results indicate that the low cost ceramic membranes represent a promising alternative to conventional water treatment methods due to their low chemical consumption, clean operation, and suitability for industrial applications.

Acknowledgements

The authors express their sincere gratitude to the Departments of Chemical and Civil Engineering, College of Engineering, University of Al-Qadisiyah, for providing laboratory facilities, technical support, and resources necessary to carry out this study.

References

1. Tang, T., W. Fu, and X. Zhang, Numerical simulation of fluid flow and desalination effects in ceramic membrane channels. Desalination, 2021. **519**: p. 115304.
2. Maguire, N.A.P., et al., Influence of Ceramic Membrane Surface Characteristics on the Flux Behavior of a Complex Fermentation Broth. Membranes (Basel), 2021. **11**(6).
3. Li, Y., et al., An effective way in application of coagulants for more accurate fouling control via transparent exopolymer particles (TEP) determination. Separation and Purification Technology, 2022. **303**: p. 122279.
4. Uyak, V., et al., Natural organic matter removal and fouling in a low pressure hybrid membrane systems. ScientificWorldJournal, 2014. **2014**: p. 893203.
5. Almasri, D., et al., A novel, low-cost clay ceramic membrane for the separation of oil-water emulsions. Sci Rep, 2025. **15**(1): p. 14457.
6. Zhang, R., et al., Quorum sensing on the activated performances of gravity-driven membrane (GDM) system at low temperatures: Ammonia removal and flux stabilization. Separation and Purification Technology, 2025. **358**: p. 130238.
7. Xiao, L., et al., Fabrication of anti-fouling and self-cleaning PHI modified PVDF membranes for high-flux dye removal††Electronic supplementary information (ESI) available. See DOI: https://doi.org/10.1039/d5ra00279f. RSC Advances, 2025. **15**(12): p. 9141-9152.
8. Jlassi, O., S. Louhichi, and S. Khemakhem, Development of a ceramic membrane on a flat support for the treatment of an industrial effluent. Desalination and Water Treatment, 2023. **313**: p. 49-56.
9. Liu, L., et al., Treatment of sewage sludge hydrothermal carbonization aqueous phase by Fe(II)/CaO2 system: Oxidation behaviors and mechanism of organic compounds. Waste Management, 2023. **158**: p. 164-175.

10. Roduner, E. and T.P.J. Krüger, The origin of irreversibility and thermalization in thermodynamic processes. Physics Reports, 2022. **944**: p. 1-43.

11. Chang, Z.H., et al., Integrated ultrafiltration-like forward osmosis and nanofiltration for natural rubber skim latex concentration: Dewatering performance, fouling mechanism, and economic analysis. Chemical Engineering Journal, 2025. **519**: p. 165024.

12. Wei, H., et al., The future of freshwater access: functional material-based nano-membranes for desalination. Materials Today Energy, 2021. **22**: p. 100856.
13. Cheng, X., et al., Investigation on operational parameters and membrane fouling performance in treating synthetic aquaculture wastewater via forward osmosis with sucrose as draw solution. Science of The Total Environment, 2022. **847**: p. 157573.
14. Xiao, X., et al., Enhancing anti-scaling and anti-fouling performance in membrane distillation through liquid-infused membrane with slippery surface and gating properties. Applied Surface Science, 2025. **707**: p. 163617.
15. Wandji Djouonkep, L.D., et al., Enhanced amphoteric polymer filtration reducer with vinyl-functionalized nanosilica for high-salt and ultra-high temperature water-based drilling environments. Geoenergy Science and Engineering, 2024. **236**: p. 212743.
16. Klima, K.M., et al., Effects of mineral wool waste in alkali activated-artificial aggregates for high-temperature applications. Construction and Building Materials, 2023. **401**: p. 132937.
17. Elomari, H., et al., Elaboration and characterization of flat membrane supports from Moroccan clays. Application for the treatment of wastewater. Desalination and Water Treatment, 2016. **57**(43): p. 20298-20306.
18. Wang, M., et al., Constructing early childhood leadership models in China: a mixed-methods study. Journal of Educational Administration, 2019. **58**(6): p. 729-748.
19. Zuo, Y., et al., Performance assessment of grid-forming and grid-following converter-interfaced battery energy storage systems on frequency regulation in low-inertia power grids. Sustainable Energy, Grids and Networks, 2021. **27**: p. 100496.
20. Shao, X., et al., Effects of Salt-Alkaline Stress on Carbohydrate Metabolism in Rice Seedlings. Phyton-International Journal of Experimental Botany, 2021. **91**(4): p. 745-759.
21. Zuo, B., et al., Identification of novel biomarkers and candidate small molecule drugs in rheumatoid arthritis and osteoarthritis based on bioinformatics analysis of high-throughput data. Bioscience Reports, 2020. **40**(12).
22. Talidi, A., et al., Manufacture and characterization of flat microfiltration membrane based on Moroccan pyrophyllite clay for pretreatment of raw seawater for desalination. Desalination and Water Treatment, 2022. **253**: p. 24-38.
23. Nath, B., et al., An investigation of thermal decomposition behavior and combustion parameter of pellets from wheat straw and additive blends by thermogravimetric analysis. International Journal of Thermofluids, 2024. **22**: p. 100660.
24. Zhang, T., et al., Biomass waste-enabled porous raw clay composites for efficient pollutant removal. Applied Surface Science, 2025. **709**: p. 163852.
25. Dorokhov, V.V., et al., Physical characteristics and combustion behavior of pellets from sawdust and refuse-derived fuel. Fuel, 2024. **377**: p. 132810.

26. Liang, D., et al., Influencing factors on the performance of tubular ceramic membrane supports prepared by extrusion. Ceramics International, 2021. **47**(8): p. 10464-10477.
27. Sharif, S.S., et al., Thermodynamics analysis and experimental investigation of EAF slag based ceramics materials for circular economy. Ceramics International, 2024. **50**(20, Part B): p. 40058-40068.
28. Reddy, B.S., et al., Enhancing structural integrity and cycle life of sulfur electrodes for Li-S batteries through an eco-friendly water-soluble binder. Journal of Alloys and Compounds, 2025. **1038**: p. 182798.
29. Mahdi, N.M. and A.H. Ali, Artificial neural network for modeling and prediction of selected dye removal and voltage generation from aqueous solution using microbial fuel cell. Desalination and Water Treatment, 2022. **252**: p. 420-436.
30. Achiou, B., et al., Manufacturing of tubular ceramic microfiltration membrane based on natural pozzolan for pretreatment of seawater desalination. Desalination, 2017. **419**: p. 181-187.
31. Xu, B., et al., A Review of Temperature Effects on Membrane Filtration. Membranes (Basel), 2023. **14**(1).
32. Ismael, B.H., et al., Permeation Flux Prediction of Vacuum Membrane Distillation Using Hybrid Machine Learning Techniques. Membranes (Basel), 2023. **13**(12).
33. Xie, Y., et al., Membrane Fouling Control and Treatment Performance Using Coagulation-Tubular Ceramic Membrane with Concentrate Recycling. Membranes (Basel), 2025. **15**(8).
34. Al-Tamimi, N.J., A.F. Al-Alawy, and M. Al-Shaeli, Process efficiency assessment of turbidity removal from tigris river using microfiltration membranes. Desalination and Water Treatment, 2024. **320**: p. 100879.
35. Akash, F.A., et al., Advancements in ceramic membrane technology for water and wastewater treatment: A comprehensive exploration of current utilizations and prospective horizons. Desalination and Water Treatment, 2024. **319**: p. 100569.
36. Addich, M., et al., Elaboration of innovative ceramic microfiltration membrane from natural Moroccan sand for wastewater treatment. Desalination and Water Treatment, 2022. **260**: p. 299-308.
37. Manni, A., et al., New low-cost ceramic microfiltration membrane made from natural magnesite for industrial wastewater treatment. Journal of Environmental Chemical Engineering, 2020. **8**(4): p. 103906.
38. Zare, J., et al., Eco-Friendly Superhydrophobic Modification of Low-Cost Multi-Layer Composite Mullite Base Tubular Ceramic Membrane for Water Desalination. Water, 2024. **16**(11).
39. Mouiya, M., et al., Flat ceramic microfiltration membrane based on natural clay and Moroccan phosphate for desalination and industrial wastewater treatment. Desalination, 2018. **427**: p. 42-50.
40. Rekik, S.B., et al., Development and characterization of porous membranes based on kaolin/chitosan composite. Applied Clay Science, 2017. **143**: p. 1-9.
41. Saja, S., et al., Elaboration and characterization of low-cost ceramic membrane made from natural Moroccan perlite for treatment of industrial wastewater. Journal of Environmental Chemical Engineering, 2018. **6**(1): p. 451-458.

42. Jedidi, I., et al., Preparation of a new ceramic microfiltration membrane from mineral coal fly ash: Application to the treatment of the textile dying effluents. Powder Technology, 2011. **208**(2): p. 427-432.
43. Vasanth, D., G. Pugazhenthi, and R. Uppaluri, Biomass assisted microfiltration of chromium(VI) using Baker's yeast by ceramic membrane prepared from low cost raw materials. Desalination, 2012. **285**: p. 239-244.
44. Nandi, B.K., et al., Microfiltration of mosambi juice using low cost ceramic membrane. Journal of Food Engineering, 2009. **95**(4): p. 597-605.